IEEE Access
Multidisciplinary ⋮ Rapid Review ⋮ Open Access Journal

Received 30 December 2023, accepted 1 March 2024, date of publication 18 March 2024, date of current version 28 March 2024.

Digital Object Identifier 10.1109/ACCESS.2024.3376391

RESEARCH ARTICLE

Dynamic Movement Primitives Modulation-Based Compliance Control for a New Sitting/Lying Lower Limb Rehabilitation Robot

JIE ZHOU[1], YAO SUN[1], RONG SONG[2], AND ZHE WEI[1]
[1]School of Mechanical Engineering, Shenyang University of Technology, Shenyang 110870, China
[2]School of Biomedical Engineering, Sun Yat-Sen University, Shenzhen Campus, Shenzhen 518107, China

Corresponding author: Zhe Wei (weizhe@sut.edu.cn)

This work was supported in part by the Key Science and Technology Program of Liaoning Province under Grant 2022020630-JH1/108; in part by the National Key Research and Development Program of China under Grant 2022YFE0201900; in part by the National Natural Science Foundation of China under Grant 51975386; in part by the Science and Technology Research and Development Program, China National Railway Group Company Ltd., under Grant N2022J014; in part by Shenzhen Science and Technology Research Program under Grant SGDX20210823103405040, and in part by the Natural Science Foundation of Guangdong Province under Grant 2023A1515011021.

ABSTRACT Compliant physical human-robot interaction (pHRI), as well as the accuracy and robustness of trajectory tracking, are crucial for rehabilitation robots. In this paper, a new sitting/lying lower limb rehabilitation robot, SUT-SLLRR, has been designed for patients with lower extremity motor dysfunction. A dynamic movement primitives modulation-based compliance control strategy (DMPM-CCS) has been proposed for the SUT-SLLRR. The high-level trajectory planner consists of the trajectory generator based on dynamic movement primitives (DMPs), acceleration layer modulation generator, and velocity layer modulation generator, which can reshape the reference trajectory to generate desired trajectory within a constrained joint space through pHRI. Besides, the linear active disturbance rejection controller (LADRC) is adopted as the low-level position controller to ensure that each joint can accurately and robustness track the desired trajectory under internal and external disturbances. Simulation and experimental results indicate that the proposed strategy can provide the compliant pHRI within the constrained joint space and ensure the accuracy and robustness of trajectory tracking.

INDEX TERMS Sitting/lying lower limb rehabilitation robot, compliance control, physical human-robot interaction, dynamic movement primitives, linear active disturbance rejection control.

I. INTRODUCTION

With the aggravation of aging, the number of stroke survivors is projected to reach 77 million globally by 2030 [1]. Since stroke is an acute cerebrovascular disease with a high disability rate [2], lower extremity motor dysfunction is often associated with stroke survivors, which affects their daily living activities. Rehabilitation training can help them recover lower extremity motor function or reduce the risk of several medical consequences secondary to paralysis, such as muscle atrophy [3]. Compared with traditional rehabilitation, robot-assisted rehabilitation training can reduce therapists' physical consumption, enhance rehabilitation training's intensity, and extend the training time [4]. Furthermore, clinical validation of lower limb rehabilitation robots (LLRRs) has shown that they have positive effects in facilitating stroke survivors to recover motor function [5].

Several types of LLRRs have been designed for the patients with different movement abilities [6]. They can be divided into the following three categories: wearable, suspended, and sitting/lying LLRRs. Wearable LLRRs need the patients to be able to walk independently, which can assist them in completing daily living activities, such as sit-to-stand transfer [7], flat ground walking [8], and going up and down stairs [9]. Compared to wearable LLRRs, suspended LLRRs, such as Lokomat [10], LOPES [11], and Walkbot [12], can also provide an approximate natural gait training environment. Besides, the suspension systems and other auxiliary devices

The associate editor coordinating the review of this manuscript and approving it for publication was Wonhee Kim.

can significantly reduce patient mobility requirements. However, the expensive equipment cost and large footprint make applying in households more difficult. Sitting/lying lower limb rehabilitation robots, such as MotionMaker™ [13], S-LLRR [14], and LLR-Ro [15], provide a compromise solution between applicability and price, which can assist patients in achieving single-joint and multi-joint rehabilitation training in both supine and sitting positions. Based on the above research, we hope to design a sitting/lying lower limb rehabilitation robot to assist patients in completing rehabilitation training at home.

Control strategies should be reasonably selected according to the patient's motor disability level. For patients with weak residual muscle strength, passive control strategies are usually needed to assist the affected limb in repeating training along a predefined trajectory. The proportional-integral-derivative (PID) controller is commonly used in rehabilitation robots to help patients follow the reference trajectory [16]. Since rehabilitation robots are highly nonlinear coupled dynamic systems and receive time-varying internal and external disturbances, PID controllers with model-free characteristics are challenging to guarantee tracking accuracy [17]. An adaptive neural network-based saturated controller was designed for a LLRR, in which the radial basis function neural networks and robust terms were adopted to compensate for the unknown dynamics [18]. An output-constrained controller with finite-time extended state observer was proposed for a lower limb exoskeleton, which can estimate and compensate for unmeasured joint velocity and lumped uncertainty [19]. Since the model parameters are difficult to obtain accurately by system identification, the active disturbance rejection controller (ADRC) has gradually gained attention in rehabilitation robots [20]. It can achieve accurate and robust trajectory tracking by relying on the system order. Furthermore, to simplify the control structure and reduce the number of tuning parameters, a linear active disturbance rejection controller (LADRC) was proposed based on ADRC [21]. Although the LADRC is suitable for rehabilitation robots, the passive control strategy rejects the patients' active contribution, resulting in patients being unable to participate actively in rehabilitation training.

Active control strategies are suitable for patients with residual muscle strength, which can promote their recovery by encouraging them to participate actively in rehabilitation training. Control strategies for rehabilitation robots typically include the high-level trajectory planner and the low-level position/torque controller [22]. Many active control strategies have been proposed by designing appropriate low-level position/torque controllers. Jamwal et al. proposed an interactive training paradigm based on impedance control, which can assist patients in completing various rehabilitation training modes such as isotonic training, active training, and isokinetic training by changing impedance parameters [23]. In [24], a position-constrained assist-as-needed control strategy was proposed for a knee exoskeleton, which can smoothly switch between human-dominated and robot-dominated modes based on robot assistance level metric. Compared to the above strategies, the active control strategies based on the high-level trajectory planner are more convenient to expand their application in different rehabilitation robots. Admittance control strategies can be designed efficiently by combining the admittance model and traditional position controller, which can reshape reference trajectory through physical human-robot interaction (pHRI) [25], [26]. In [25], an admittance adaptive fuzzy control strategy has been proposed for a walking exoskeleton robot, in which the integral-type Lyapunov function controller with the disturbance observer was designed to ensure tracking performance, and the admittance model was adopted to make the robot adapt to human walking intention by shaping step trajectory. In [26], a variable admittance time-delay control strategy has been developed for a planar upper limb rehabilitation robot, in which a sliding mode controller with a time-delay approximator is utilized to enhance tracking accuracy, and the admittance model with an iterative optimization algorithm is used to adjust human-robot interaction compliance based on estimated human arm stiffness. Although these admittance control strategies allow patients to participate actively in rehabilitation training, the admittance model and trajectory planner are usually independent. Meanwhile, they need to design an additional smooth constraint function to ensure the safety of pHRI [27].

In this paper, a dynamic movement primitives modulation-based compliance control strategy (DMPM-CCS) was proposed for a new self-designed sitting/lying lower limb rehabilitation robot. Simulations and experiments were performed to verify the DMPM-CCS. The main contributions of this paper can be summarized as follows:

1) A new sitting/lying lower limb rehabilitation robot was designed for patients with lower extremity motor dysfunction, which can assist knee and ankle joints in independent or collaborative rehabilitation training in the sagittal plane. Besides, the seat backrest angle, seat height, exoskeleton length, etc., can be conveniently adjusted according to the needs of different participants.
2) The DMPM-CCS was proposed based on dynamic movement primitives (DMPs) [28] and LADRC. It relies on dynamic movement primitives modulation to achieve compliant pHRI and restrict abnormal desired trajectory without needing an admittance model and soft saturation function. Besides, the LADRC was used to compensate for total disturbances and ensure the accuracy and robustness of trajectory tracking.
3) Simulations and experimental studies were conducted to verify the effectiveness of the DMPM-CCS. Results indicate that the proposed strategy can provide compliant pHRI and ensure the accuracy and robustness of trajectory tracking. Moreover, the desired trajectory can be restricted between the upper and lower boundary

trajectory, avoiding desired trajectories beyond the safe range of motion caused by abnormal interactions.

II. SYSTEM DESCRIPTION

A. STRUCTURE DESIGN OF SUT-SLLRR

As illustrated in Fig. 1 (a), we designed a sitting/lying lower limb rehabilitation robot, SUT-SLLRR, to assist knee and ankle joints in independent or collaborative rehabilitation training in the sagittal plane. Velcro straps were adapted to fasten the participant's calf and foot to the SUT-SLLRR, and the moveable bracket was designed for the convenience of robot transportation. As shown in Fig. 1 (b), the servo motor was used to drive each joint, the output shaft speed of the motor was reduced through a harmonic reducer to meet the speed and torque requirements of the rehabilitation training, and the stop ring and flange can limit the range of motion. As illustrated in Fig. 1 (c), the height of the SUT-SLLRR can be easily adjusted by a height handwheel through the worm gear assembly, leadscrew, coupling, connecting shaft, and connecting flange. It can facilitate different participants sitting on the SUT-SLLRR and adjust suitable height for rehabilitation training. As illustrated in Fig. 1 (d) and (e), the positions of the knee joint can be adjusted by the gear rack mechanism through the length handwheel, and it can be maintained using the gasket, the fixed block, and the fixed knob. Besides, the switch between sitting and lying can be achieved by adjusting the angle of the backrest through the backrest knob. Furthermore, as illustrated in Fig. 1 (f), the length of the calf exoskeleton is adjustable to fit the participants' leg length, which can be adjusted by the axial sliding of the inner and outer sliding rods, and the fixed knob and the fastening ring can be used to lock the length of the calf exoskeleton.

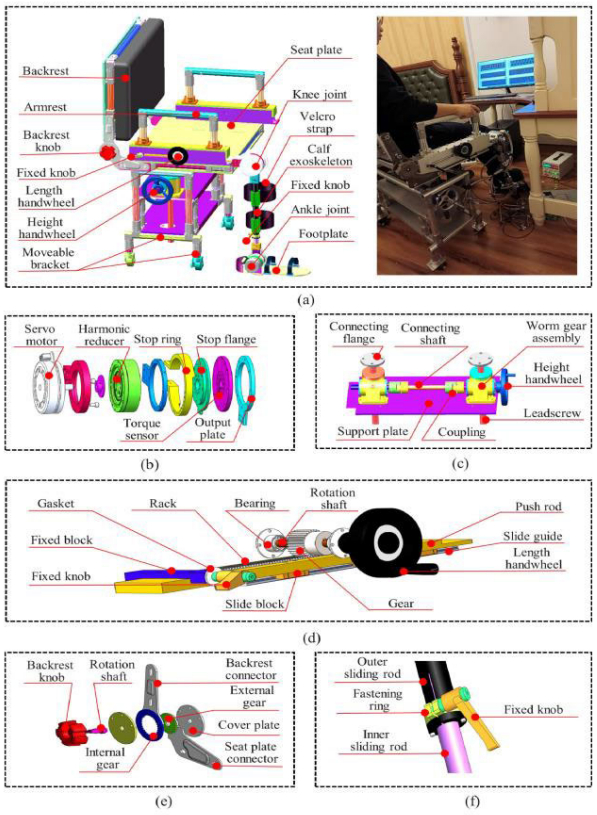

FIGURE 1. Mechanical structure of SUT-SLLRR: (a) is the virtual and actual prototype of SUT-SLLRR; (b) is mechanical structure of knee joint; (c) is the composition of the mechanism for adjusting seat height; (d) is the composition of the mechanism for adjusting the anterior and posterior positions of the knee joint; (e) is the composition of the mechanism for adjusting the angle of backrest; (f) is the composition of the mechanism for adusting and locking the length of the calf exoskeleton.

B. CONTROL SYSTEM

The control system comprises two joint actuator modules, a personal computer, and a data acquisition/output device. Like [8], the knee joint actuator module is driven by a 220 W brushless DC servo motor (EC 90 flat, Maxon, Sachseln, Switzerland). A harmonic reducer (LCD-20-100-C-I, Leader, Jiangsu, China) with a transmission ratio of 100:1 is connected to the motor, and a 150 Nm torque sensor (M2212A, SRI, Guangxi, China) is attached to measure joint torque. Besides, a 100 W brushless DC servo motor (EC 60 flat, Maxon, Sachseln, Switzerland), a harmonic reducer (LCD-17-100-C-I-ST, Leader, Jiangsu, China), and a torque sensor (M2210N4, SRI, Guangxi, China) are applied to constitute the ankle joint actuator module. The angle of each active joint is sensed using an incremental encoder (MILE 1024, Maxon, Sachseln, Switzerland) located inside the servo motor, and different servo motors are controlled by the same servo driver (Module 50/5, Maxon, Sachseln, Switzerland). The data acquisition/output device (NI DAQ, 6341, National Instruments, USA) serves as an interface between the SUT-SLLRR and a personal computer, which can collect and output signals to control the servo driver of each joint. The personal computer with the LabVIEW 2018 software can execute control strategies and provide visual feedback for the participant, as shown in Fig. 1 (a).

C. SECURITY PROTECTION

It is essential to protect participants from injury in experiments, which should be considered during the structure design and control system construction. The software-level security protection method is designed in which each joint angle can be restricted within a physiologically safe range of motion, and it can switch off the SUT-SLLRR automatically once it detects the angle beyond the safe range. Besides, the power control-level security protection method is used; the emergency shutdown buttons are provided for the operator and participant, helping them switch off the SUT-SLLRR in time under abnormal circumstances. Moreover, the mechanical structure-level security protection method is designed; if the former two protection methods fail, the stop ring and flange can limit the range of motion, which can play a final protective role for participants even in abnormal controller and sensor conditions.

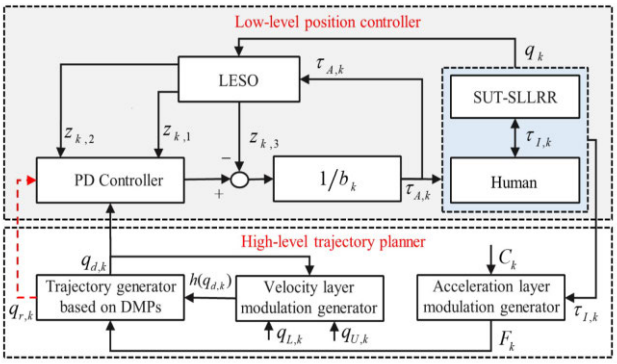

FIGURE 2. The framework of DMPM-CCS for one active joint.

III. METHOD

A. CONTROL STRATEGY FOR SUT-SLLRR

The DMPM-CCS is proposed for the SUT-SLLRR, and the control framework for one active joint is shown in Fig. 2. The proposed control strategy consists of a high-level trajectory planner and a low-level position controller. The high-level trajectory planner consists of a trajectory generator based on DMPs, an acceleration layer modulation generator, and a velocity layer modulation generator, which can generate desired trajectory within a constrained joint space through compliant pHRI. Besides, the LADRC consists of a linear extended state observer (LESO) and a proportional-derivative (PD) controller, ensuring the accuracy and robustness of trajectory tracking under internal and external disturbances.

It is worth noting that to avoid confusion between the reference trajectory and the desired trajectory, we provide the following explanation: 1) The reference trajectory for each active joint is generated by the trajectory generator based on DMPs without acceleration and velocity layer modulation; 2) The desired trajectory for each active joint is generated by the trajectory generator based on DMPs with acceleration and velocity layer modulation during pHRI.

B. TRAGJECTORY GENERATOR BASED ON DMPs

The DMPs have good ability of motion learning and motion generalization, which is useful for encoding and adjusting the periodic reference trajectory [29]. For the k_{th} joint of the SUT-SLLRR ($k = 1$ and $k = 2$ represent the knee and ankle joints, respectively), the trajectory generator is defined by nonlinear differential equations, and the transformation system of the DMPs is given as follows:

$$\kappa \dot{z}_{\mathrm{r},k} = \alpha(\beta(g_{\mathrm{r},k} - q_{\mathrm{r},k}) - z_{\mathrm{r},k}) + f_{\mathrm{r},k}(\phi, r), \tag{1}$$

$$\kappa \dot{q}_{\mathrm{r},k} = z_{\mathrm{r},k}, \tag{2}$$

Here, $f_{r,k}(\phi, r)$ is defined as a linear combination of nonlinear basis functions

$$f_{\mathrm{r},k}(\phi, r) = \frac{\sum_{i=1}^{m} \psi_i(\phi) w_{\mathrm{r},k,i}}{\sum_{i=1}^{m} \psi_i(\phi)} r, \tag{3}$$

$$\psi_i(\phi) = \exp\left(\frac{\cos(\phi - c_i) - 1}{2\sigma_i^2}\right), \tag{4}$$

where κ is the positive temporal scaling factor; a smaller temporal scaling factor value indicates that periodic reference trajectory has higher frequency; α and β are positive constants to ensure that the transformation system is in a critical damping state; $g_{\mathrm{r},k}$ is the position goal; $f_{\mathrm{r},k}(\phi, r)$ is the forcing term obtained by supervised learning; we adopt the locally weighted regression method [28] in this article; $q_{\mathrm{r},k}$ and $\dot{q}_{\mathrm{r},k}$ are the reference angle and angular velocity; $z_{\mathrm{r},k}$ and $\dot{z}_{\mathrm{r},k}$ are the reference angular velocity and angular acceleration after expansion or contraction; ϕ is phase variable; ψ_i is the i_{th} kernel function; σ_i and c_i are constants that determine the width and center of the i_{th} kernel function; m is the number of kernel functions; $w_{k,i}$ is the weight coefficient corresponding to the kernel function ψ_i.

The canonical system of the DMPs of is introduced as follows to solve the time-dependence problem of forcing term

$$\kappa \dot{\phi} = 1, \tag{5}$$

where ϕ is the phase variable, whose initial and final values are 0 and 1, respectively. Besides, we introduce the following equation to achieve smooth adjustment of trajectory amplitude

$$\kappa \dot{r} = \alpha_{\mathrm{r}}(r_0 - r), \tag{6}$$

where r_0 is the amplitude modulation factor, a smaller amplitude modulation factor value indicates that the periodic reference trajectory has higher amplitude; r is the state variable of amplitude modulation factor; α_{r} is a positive constant that determines the speed of amplitude modulation factor change.

C. DYNAMIC MOVEMENT PRIMITIVES MODULATION

It is worth noting that the DMPs can be modulated online and respond in real-time to dynamic events occurring in the environment [30]. As a result, it becomes crucial to implement the acceleration and velocity layer modulation to ensure that physical human-robot interaction is compliant and abnormal desired trajectory can be restricted.

The transformation system of the DMPs after the acceleration layer modulation is given as follows:

$$\kappa \dot{z}_{\mathrm{d},k} = \alpha(\beta(g_{\mathrm{d},k} - q_{\mathrm{d},k}) - z_{\mathrm{d},k}) + f_{\mathrm{d},k}(\phi, r), \tag{7}$$

$$f_{\mathrm{d},k}(\phi, r) = f_{\mathrm{r},k}(\phi, r) + F_k, \tag{8}$$

$$F_k = C_k \hat{\tau}_k, \tag{9}$$

$$\hat{\tau}_k = \begin{cases} \tau_k, & |\tau_k| \geq \bar{\tau}_k \\ 0, & |\tau_k| < \bar{\tau}_k, \end{cases} \tag{10}$$

where $q_{\mathrm{d},k}$ is the desired angle for the k_{th} joint during physical human-robot interaction; $f_{\mathrm{d},k}(\phi, r)$ is the forcing term after the acceleration layer modulation; F_k is the modulation term; C_k is the sensitivity factor, a smaller sensitivity factor value indicates the lower robot compliance; τ_k is the interaction torque from the torque sensor; $\hat{\tau}_k$ represents the interaction torque after truncation processing; $\bar{\tau}_k$ represents the interaction torque threshold, which is the minimum interaction

torque required for activating the spatial modulation of the DMPs at the acceleration level. Besides, the transformation system of the DMPs after the velocity layer modulation is given as follows:

$$\kappa \dot{q}_{\mathrm{d},k} = z_{\mathrm{d},k} + h(q_{\mathrm{d},k}), \tag{11}$$

$$h(q_{\mathrm{d},k}) = -\frac{1}{\gamma}\left(\frac{1}{(q_{\mathrm{L},k} - q_{\mathrm{d},k})^3} + \frac{1}{(q_{\mathrm{U},k} - q_{\mathrm{d},k})^3}\right), \tag{12}$$

where $\dot{q}_{d,k}$ is the desired angular velocity; $h(q_{d,k})$ is the repulsive force function; γ is the repulsive force factor; $q_{\mathrm{L},k}$ and $q_{\mathrm{U},k}$ are the upper and lower boundaries of the desired trajectory, respectively.

D. LADRC

Although achieving compliant pHRI and restricting abnormal desired trajectory is crucial for enhancing patient engagement and safety, the accuracy and robustness of trajectory tracking are the foundation for rehabilitation training. In this part, the LADRC is adopted to ensure each joint tracks the desired trajectory under internal and external disturbances.

The dynamic model of k_{th} joint in the human-robot coupling system can be simplified as follows:

$$\begin{aligned} &J_k\ddot{q}_k + B_k\dot{q}_k + G_k\sin(q_k) + T_k sgn(\dot{q}_k) \\ &= \tau_{\mathrm{A},k} + \tau_{\mathrm{E},k} + \tau_{\mathrm{H},k}, \end{aligned} \tag{13}$$

where J_k is the inertial of the robotic exoskeleton (including the participant's leg); B_k is the viscous friction torque coefficient; G_k is the gravity torque; T_k is the Coulomb friction torque; $\tau_{\mathrm{A},k}$ is the control torque; $\tau_{\mathrm{H},k}$ is the active joint torque of participants; $\tau_{\mathrm{E},k}$ is the external disturbances.

Equation (13) can be rewritten as follows:

$$\ddot{q}_k = f_k + b_k\tau_{\mathrm{A},k}, \tag{14}$$

$$\begin{aligned} f_k = &\frac{1}{J_k}(\tau_{\mathrm{E},k} + \tau_{\mathrm{H},k} - B_k\dot{q}_k - G_k\sin(q_k) \\ &- T_k\mathrm{sgn}(\dot{q}_k)) + (\frac{1}{J_k} - b_k)\tau_{\mathrm{A},k}, \end{aligned} \tag{15}$$

where f_k is the total disturbances consisting of internal and external disturbances; b_k is the compensation factor determined by dynamic characteristics. We defined the state variable to $x_{k,1} = q_k, x_{k,2} = \dot{q}_k, x_{k,3} = f_k$, and the state space form of (14) can be given as follows:

$$\begin{cases} \dot{\mathbf{x}}_k = \mathbf{A}\mathbf{x}_k + \mathbf{B}_k\tau_{\mathrm{A},k} + \mathbf{E}\dot{f}_k \\ q_k = \mathbf{C}x_k, \end{cases} \tag{16}$$

where $\mathbf{x}_k = [q_k, \dot{q}_k, f_k]$ is the extended state vector, and

$$\mathbf{A} = \begin{bmatrix} 0 & 1 & 0 \\ 0 & 0 & 1 \\ 0 & 0 & 0 \end{bmatrix}, \mathbf{B}_k = \begin{bmatrix} 0 \\ b_k \\ 0 \end{bmatrix}, \mathbf{E} = \begin{bmatrix} 0 \\ 0 \\ 1 \end{bmatrix}, \mathbf{C} = \begin{bmatrix} 1 & 0 & 0 \end{bmatrix}.$$

Then, the continuous linear extended state observation to (16) can be given as follows:

$$\begin{cases} \dot{\mathbf{z}}_{\mathrm{o},k} = [\mathbf{A} - \mathbf{L}_k\mathbf{C}]\mathbf{z}_{\mathrm{o},k} + [\mathbf{B}, \mathbf{L}_k]\mathbf{D}_k \\ \boldsymbol{\theta}_k = \mathbf{z}_{\mathrm{o},k}, \end{cases} \tag{17}$$

where $\mathbf{z}_{\mathrm{o},k} \rightarrow \mathbf{x}_k$, and $\mathbf{z}_{\mathrm{o},k}$ is the state vector of LESO; $\mathbf{L}_k$ is the observer error feedback gain vector; $D_k = [\tau_{\mathrm{A},k}, q_k]^T$ is the combining input vector; $\boldsymbol{\theta}_k = [\hat{q}_k, \hat{\dot{q}}_k, \hat{f}_k]$ is the output vector.

It is worth noting that the observer error feedback gain matrix needs to be designed reasonably to achieve satisfactory observation results. The poles of the observer's characteristic equation are set at the same position on the left side of the complex plane, i.e., $\mathbf{L}_k = \left[3\omega_{\mathrm{o},k}, 3\omega_{\mathrm{o},k}^2, \omega_{\mathrm{o},k}^3\right]$, and it follows that

$$\lambda_k(s) = |s\mathbf{I} - (\mathbf{A} - \mathbf{L}\mathbf{C})| = (s + \omega_{\mathrm{o},k})^3, \tag{18}$$

where $\mathbf{I} \in \mathbb{R}^{3\times3}$ is an identity matrix, and $\omega_{\mathrm{o},k}$ is the observer bandwidth of LESO.

Since the LESO can estimate the external and internal disturbances in real time, the integrator term used to eliminate steady state errors in classical PID is unnecessary. Thus, the linear state feedback control law for the k_{th} joint of the SUT-SLLRR can be described as follows:

$$\tau_{\mathrm{A},k} = \frac{k_{\mathrm{p},k}(q_{\mathrm{d},k} - q_k) - k_{\mathrm{d},k}\dot{q}_k - \hat{f}_k}{b_k}, \tag{19}$$

where $k_{\mathrm{p},k} = \omega_{\mathrm{c},k}^2$ and $k_{\mathrm{d},k} = 2\omega_{\mathrm{c},k}$ are the proportional and derivative gain; $\omega_{\mathrm{c},k}$ is the controller bandwidth; $q_{\mathrm{d},k}$ and $\dot{q}_{\mathrm{d},k}$ are the desired angle and angular velocity during pHRI. The stability analysis of the LADRC for nonlinear systems with dynamic uncertainties has been considered in [31].

IV. SIMULATIONS AND EXPERIMENTS

A. SIMULATION STUDIES

1) SIMULATION SETTING

Compliant pHRI verification of DMPM-CCS was carried in MATLAB under different sensitivity factors ($C_1 = 1, C_1 = 2$, and $C_1 = 3$), simulation and sample time were set to 30 s and 0.01 s, respectively. The parameters of the DMPs were set as follows: $\alpha = 25, \beta = 6.25, \alpha_{\mathrm{r}} = 12.5, g_{\mathrm{r},1} = 0, g_{\mathrm{d},1} = 0, \kappa = 1$ and $r_0 = 0.9$. Besides, the interaction torque threshold, the repulsive force factor, the upper and lower boundaries of the desired trajectory for knee joint were set to $\bar{\tau}_1 = 4$Nm, $\gamma = 1000000$, $q_{\mathrm{L},1} = -0.15$rad, and $q_{\mathrm{U},1} = 1.0$ rad. Similar to [32], the dynamic parameters of the knee joint were set as follows: $J_1 = 0.35, B_1 = 0.486, G_1 = 13.55$, and $T_1 = 3.33$. For the LADRC, the compensation factor, the observer bandwidth, the controller bandwidth were set to $b_1 = 3.5, w_{\mathrm{o},1} = 105$, and $w_{\mathrm{c},1} = 35$. To better mimic the active torque applied by the human body, according to [33], the following interaction torque was set to simulate the active torque applied by the participants:

$$\begin{aligned} \bar{\tau}_{\mathrm{H},1}(t) = &a_1\sin(\frac{b_1 t}{10} + c_1) + a_2\sin(\frac{b_2 t}{10} + c_2) \\ &+ a_3\sin(\frac{b_3 t}{10} + c_3) + a_4\sin(\frac{b_4 t}{10} + c_4) \\ &+ a_5\sin(\frac{b_5 t}{10} + c_5), \end{aligned} \tag{20}$$

$$\tau_{\mathrm{H},1}(t) = \begin{cases} \bar{\tau}_{\mathrm{H},1}(t-10), & 10 \le t \le 23.5 \\ 0, & otherwise, \end{cases} \tag{21}$$

The fitting parameters were set as follows:

$$\begin{aligned} &\mathrm{a}_1 = 60.91, b_1 = 0.4741, c_1 = -0.2221, \mathrm{a}_2 = 8.315, \\ &b_2 = 11.22, c_2 = -4.447, \mathrm{a}_3 = 23.17, b_3 = 13.14, \\ &c_3 = -2.834, \mathrm{a}_4 = 17.32, b_4 = 13.87, c_4 = -0.2997, \\ &\mathrm{a}_5 = 26.16, b_5 = 2.786, c_5 = 0.7481. \end{aligned}$$

2) SIMULATION RESULTS

From Fig. 3 (a), the DMPs can be modulated online through interaction torque, which can continuously generate the desired trajectory when pHRI occurs, and the desired trajectory gradually converges back to the reference trajectory once pHRI stops. Meanwhile, increasing the sensitivity factor enhances the deviation between the desired and reference trajectories under the same interaction torque. Besides, the desired trajectory can be restricted between the upper and lower boundary trajectories, ensuring it stays within a safe range of motion. In Fig. 3 (b), the control torque is smooth, except for near-sudden changes in interaction torque. The size and shape of the control torque are similar to the control torque generated by the state observer, indicating that the LESO can effectively compensate for internal and external disturbances. Furthermore, the control torque generated by PD is minimal under different sensitivity factors, suggesting that the precise feedforward compensation from LESO significantly weakens the contribution of feedback control.

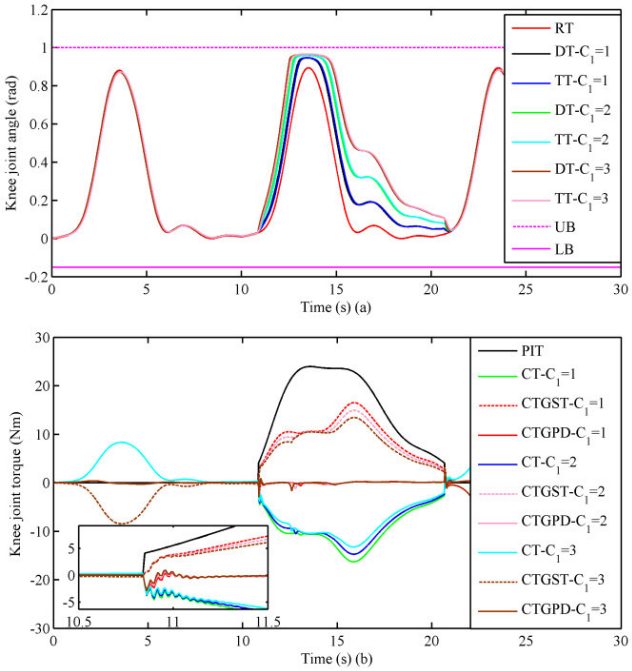

FIGURE 3. Results of the compliant pHRI verification in knee joint: (a) is the compliant pHRI performance of DMPM-CCS; (b) is the control toruqe of DMPM-CCS under preset interaction torque. RT, DT, TT, UB, and LB represent reference trajectory, desired trajectory, tracking trajectory, upper boundary trajectory, and lower boundary trajectory, respectively. PIT, CT, CTGSO, and CTGPD represent preset interaction torque, control torque, control torque generated by state observer, and control torque generated by PD, respectively.

B. EXPERIMENTAL STUDIES

1) EXPERIMENTAL SETTING

We carried out the robustness and compliant pHRI verification experiments on the SUT-SLLRR. In the robustness verification experiment, we bound 1 kg, 2 kg, and 4 kg weights at the footplate to simulate different loads and conducted three trials under each load condition. Besides, the compliant pHRI verification experiment was carried out on one healthy participant, who was required to apply active torque during the experiment. Similar to the robustness verification experiment, we conducted three trials. We evaluated trajectory tracking performance using average error, excluding the first and last cycles.

Control parameters should be set reasonably. For robustness verification experiment, the sensitivity factor for each joint was set to $C_1 = C_2 = 0$, the compensation factor, the observer bandwidth, the controller bandwidth were set to $b_1 = 8, b_2 = 10, w_{\mathrm{o},1} = 25, w_{\mathrm{o},2} = 30, w_{\mathrm{c},1} = 25$, and $w_{\mathrm{c},2} = 30$. Other parameters of the DMPM-CCS were set the same as that in simulation. For compliant pHRI verification experiment, the sensitivity factor for each joint was set to $C_1 = 2$ and $C_2 = 1$, the interaction torque threshold were set to $\bar{\tau}_1 = 2$ Nm and $\bar{\tau}_2 = 2$ Nm, the upper and lower boundaries of the desired trajectory for knee and ankle joints were set to $q_{\mathrm{L},1} = -0.15$ rad, $q_{\mathrm{U},1} = 1.0$ rad, $q_{\mathrm{L},2} = -0.3$ rad, and $q_{\mathrm{U},2} = 0.3$ rad. Other parameters were set the same as that in robustness verification experiment.

2) EXPERIMENTAL RESULTS

Fig. 4 (a) and (b) demonstrate that the trajectory generator based on DMPs can generate continuous periodic reference trajectories for knee and ankle joints. The tracking trajectory of each joint can accurately follow the reference trajectory, even when a 4 kg load weight is placed on the footplate. Additionally, the maximum tracking errors of the knee and ankle joints are less than 0.08 rad and 0.04 rad, respectively. As seen in Fig. 4 (c), the knee and ankle joint observation torques are smooth and show clear periodic characteristics, ranging from −80 to 50 Nm and −40 to 40 Nm, respectively. In Fig. 4 (d), the ankle joint duty cycle is smaller than the knee joint, which is in line with the observation torque.

In Fig. 5 (a) and (b), the trajectory generator based on DMPs can reshape the reference trajectory, thereby producing the desired trajectory for the knee joint during physical interaction. Once the interaction torque reduces to a small range, the desired trajectory gradually converges to the reference trajectory. Even though the interaction torque exceeds 15 Nm, the desired trajectory lies within the upper and lower boundaries, consistent with the simulation results. Furthermore, due to the application of active torque by the participant, the amplitude of the knee joint duty cycle is larger than

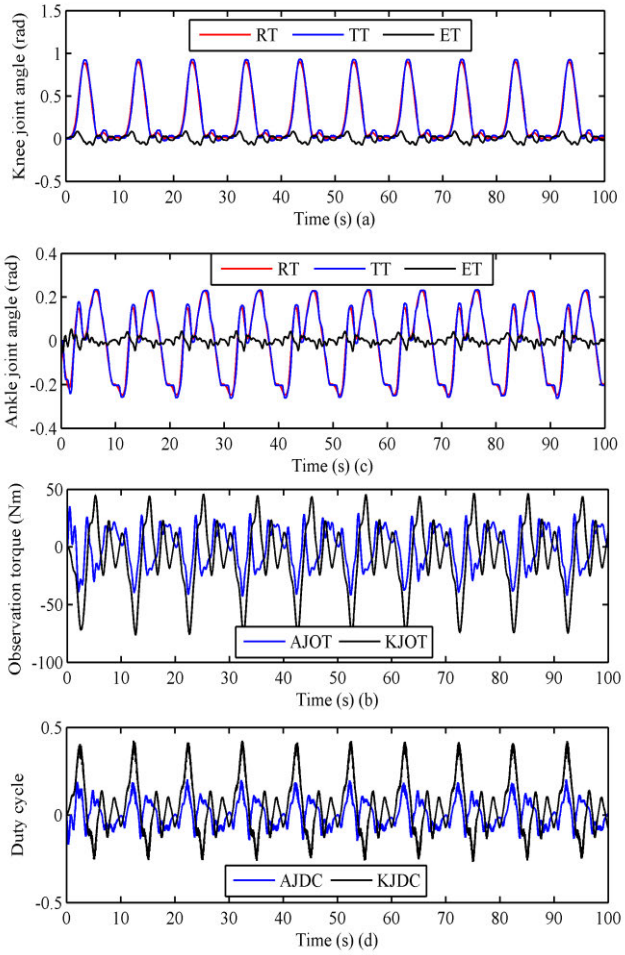

FIGURE 4. Results of the robustness verification experiment with 4 kg load weight. The RT, TT, and ET represent reference trajectory, tracking trajectory, and error trajectory, respectively. The AJOT, KJOT, AJDC, and KJDC represent ankle joint observation torque, knee joint observation torque, ankle joint duty cycle, and knee joint duty cycle, respectively.

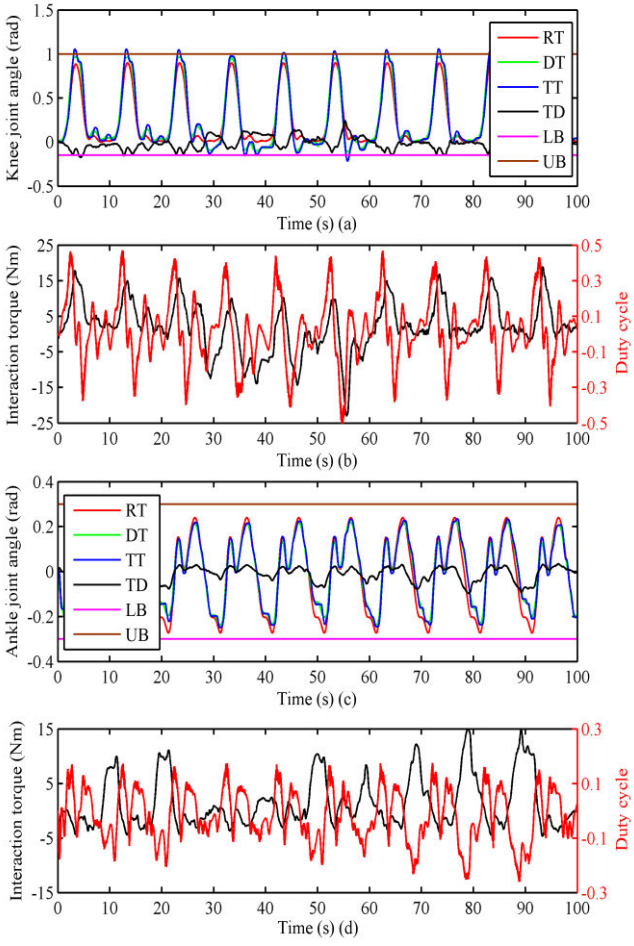

FIGURE 5. Results of the compliant pHRI verification experiment with one healthy participant. The RT, DT, TT, UB, and LB represent reference trajectory, desired trajectory, tracking trajectory, upper boundary trajectory, and lower boundary trajectory, respectively. TD represents the trajectory deviation between the desired trajectory and the reference trajectory.

that shown in Fig. 4 (d). In Fig. 5 (c) and (d), compared to the knee joint, the tracking trajectory of the ankle joint can more accurately follow the desired trajectory due to the smaller interaction torque. Additionally, from 30 s to 100 s, the trajectory deviation gradually increases with the increase of interaction torque, and there is a slight chattering in the duty cycle.

Table 1 shows the quantitative analysis results when using the DMPM-CCS. During the robustness verification experiment, the mean average error for the ankle joint is only 0.0137 rad when a 1 kg load weight is applied on the footplate, and it remains relatively unchanged even as the load weight is increased to 4 kg. However, compared with the ankle joint, the mean average error of the knee joint under different load weights increased significantly, reaching 132.85% (1 kg), 136.76% (2 kg), and 143.07% (4 kg). Moreover, the mean average error of both the knee and ankle joints increases when subjected to the compliant pHRI verification experiment. Specifically, compared to results when the load weight is set to 4 kg, the mean average error of the ankle joint increases by 8.76%, while that of the knee joint increases by 13.51%. It is worth noting that the maximum average error of the knee and ankle joints is 0.0379 rad and 0.0153 rad, respectively, which is well within the acceptable range for trajectory tracking in rehabilitation training.

V. DISCUSSION

A. COMPLIANT PHRI IN CONSTRAINED JOINT SPACE

Compliant pHRI is crucial for enhancing patient engagement and safety during rehabilitation training. In this article, the DMPs modulation method is used to design the trajectory generator that considers the interaction torque and constrained joint space, thereby achieving safe and compliant pHRI [30]. The DMPs can be used to learn the reference trajectory for each joint using the locally weighted regression method [28] and generalize the reference trajectory by adjusting the temporal scaling factor and amplitude modulation factor [8]. Besides, the spatial modulation of the DMPs at

TABLE 1. Results of experiments.

Experiment category	Load weight/active torque	Active Joint	Average error (rad)			Statistical results	
			NO.1	NO.2	NO.3	Mean	Variance
Robustness verification experiment	1 kg	Ankle	0.0138	0.0136	0.0138	0.0137	1.0977×10^{-8}
	Without active torque	Knee	0.0319	0.0321	0.0316	0.0319	5.5799×10^{-8}
	2 kg	Ankle	0.0136	0.0136	0.0137	0.0136	6.3543×10^{-9}
	Without active torque	Knee	0.0323	0.0323	0.0320	0.0322	2.5785×10^{-8}
	4 kg	Ankle	0.0135	0.0138	0.0140	0.0137	4.9877×10^{-8}
	Without active torque	Knee	0.0333	0.0333	0.0332	0.0333	6.0414×10^{-9}
Compliant pHRI verification experiment	Healthy participant	Ankle	0.0153	0.0149	0.0146	0.0149	1.4220×10^{-7}
	With active torque	Knee	0.0375	0.0379	0.0379	0.0378	4.7617×10^{-8}

the acceleration level is adopted to realize compliant pHRI. The sensitivity factor is similar to the admittance gain in [22]; increasing its value can enhance robot compliance. Additionally, within a suitable range, the sensitivity factor can ensure pHRI stability, as the transformation system of the DMPs is a second-order critical damping system. Moreover, the spatial modulation of the DMPs at the velocity level is implemented to prevent the desired trajectory from exceeding the safety range in joint space. Compared to [8] and [27], it can restrict the desired trajectory within a safe joint space without designing a soft saturation function. While the actual joint position depends on the position controller, spatial constraints on the desired trajectory can be beneficial for ensuring the safety of rehabilitation training.

B. ACCURATE AND ROBUST TRAJECTORY TRACKING

Ensuring the accuracy and robustness of trajectory tracking is the foundation for rehabilitation training. Since the unexpected behavior of stroke patients, model uncertainties, and external disturbances [34], [35], how to easily and effectively achieve accurate and robust trajectory tracking remains a challenge. In this article, the LADRC consists of the LESO and the PD controller is adopted to ensure each joint accurately tracking reference/desired trajectory. Although many model-based controllers, such as the adaptive sliding-mode controller [36] and the adaptive robust controller [37], have been proposed to enhance the anti-disturbance ability of rehabilitation robots. Furthermore, radial basis function neural networks [18], finite-time extended state observer [19], and nonlinear disturbance observer [38] are also embedded in model-based controllers to strengthen the anti-disturbance ability. However, the model parameters of the coupling model are difficult to obtain accurately by system identification, and controller design and parameter tuning are time-consuming. In contrast, the LADRC inherits the model-free characteristics of PID controllers and ensure the accuracy and robustness of trajectory tracking [39]. Besides, the parameter tuning of LADRC was more straightforward than that of the above model-based controllers, and only three main parameters (the compensation factor, the controller bandwidth, and the observer bandwidth) to be tuned [21].

C. LIMITATIONS AND FUTURE WORK

This article has several limitations that should be addressed in future research. Firstly, the torque sensor used to extract motion intention is prone to several interferences, such as gravity torque, friction torque, inertial torque, and passive joint torque [32], which has impact on motion intention extraction and human-robot synchronization [40]. To overcome this limitation, the electromyography (EMG)-driven musculoskeletal model [41] and muscle synergy-driven adaptive network approach [42] will be applied to estimate active joint torque. Secondly, although passive and active training for participants can achieved by setting different sensitivity factors, which may not be applicable to match the varying motor abilities of different participants. Similar to [43] and [44], the multi-modal adaptive control strategy based on a motion intention and motion performance will be developed, helping the SUT-SLLRR match varying motor abilities. Thirdly, although the spatial constraints on the desired trajectory are essential, the position controller with output and velocity constraints will also be used to enhance the safety of rehabilitation training [45]. Finally, robot-assisted experiments were performed on the healthy participant, a patients-based experiment will be carried out on the SUT-SLLRR to verify the clinical effectiveness of the DMPM-CCS.

VI. CONCLUSION

In this study, we design a new sitting/lying lower limb rehabilitation robot, named SUT-SLLRR, and propose a control strategy, called DMPM-CCS, for the SUT-SLLRR. Simulation and experimental studies were conducted to verify the effectiveness of the DMPM-CCS. The results indicate that the proposed control strategy can generate desired trajectory within a constrained joint space through pHRI, while ensuring the accuracy and robustness of trajectory tracking. These findings demonstrate that the DMPM-CCS has immense potential to be used in various fields involving pHRI, especially in rehabilitation robots.

REFERENCES

[1] D. Mukherjee and C. G. Patil, "Epidemiology and the global burden of stroke," *World Neurosurgery*, vol. 76, no. 6, pp. 85–90, Dec. 2011, doi: 10.1016/j.wneu.2011.07.023.

[2] A. V. Vasiliadis and M. Zikić, "Current status of stroke epidemiology in greece: A panorama," *Neurologia Neurochirurgia Polska*, vol. 48, no. 6, pp. 449–457, Nov. 2014, doi: 10.1016/j.pjnns.2014.11.001.

[3] B. Chen, H. Ma, L.-Y. Qin, F. Gao, K.-M. Chan, S.-W. Law, L. Qin, and W.-H. Liao, "Recent developments and challenges of lower extremity exoskeletons," *J. Orthopaedic Transl.*, vol. 5, pp. 26–37, Apr. 2016, doi: 10.1016/j.jot.2015.09.007.

[4] G. Colombo, M. Joerg, R. Schreier, and V. Dietz, "Treadmill training of paraplegic patients using a robotic orthosis," *J. Rehabil. Res. Dev.*, vol. 37, pp. 693–700, Nov. 2000.

[5] Y. Li, T. Fan, Q. Qi, J. Wang, H. Qiu, L. Zhang, X. Wu, J. Ye, G. Chen, J. Long, Y. Wang, G. Huang, and J. Li, "Efficacy of a novel exoskeletal robot for locomotor rehabilitation in stroke patients: A multi-center, non-inferiority, randomized controlled trial," *Frontiers Aging Neurosci.*, vol. 13, Aug. 2021, Art. no. 706569, doi: 10.3389/fnagi.2021.706569.

[6] S. Qiu, Z. Pei, C. Wang, and Z. Tang, "Systematic review on wearable lower extremity robotic exoskeletons for assisted locomotion," *J. Bionic Eng.*, vol. 20, no. 2, pp. 436–469, Mar. 2023, doi: 10.1007/s42235-022-00289-8.

[7] A. Tsukahara, R. Kawanishi, Y. Hasegawa, and Y. Sankai, "Sit-to-stand and stand-to-sit transfer support for complete paraplegic patients with robot suit HAL," *Adv. Robot.*, vol. 24, no. 11, pp. 1615–1638, Jan. 2010, doi: 10.1163/016918610x512622.

[8] J. Zhou, H. Peng, S. Su, and R. Song, "Spatiotemporal compliance control for a wearable lower limb rehabilitation robot," *IEEE Trans. Biomed. Eng.*, vol. 70, no. 6, pp. 1858–1868, Jun. 2022, doi: 10.1109/TBME.2022.3230784.

[9] Z. Li, C. Deng, and K. Zhao, "Human-cooperative control of a wearable walking exoskeleton for enhancing climbing stair activities," *IEEE Trans. Ind. Electron.*, vol. 67, no. 4, pp. 3086–3095, Apr. 2020, doi: 10.1109/TIE.2019.2914573.

[10] R. Riener, L. Lunenburger, S. Jezernik, M. Anderschitz, G. Colombo, and V. Dietz, "Patient-cooperative strategies for robot-aided treadmill training: First experimental results," *IEEE Trans. Neural Syst. Rehabil. Eng.*, vol. 13, no. 3, pp. 380–394, Sep. 2005, doi: 10.1109/TNSRE.2005.848628.

[11] J. F. Veneman, R. Kruidhof, E. E. G. Hekman, R. Ekkelenkamp, E. H. F. van Asseldonk, and H. van der Kooij, "Design and evaluation of the LOPES exoskeleton robot for interactive gait rehabilitation," *IEEE Trans. Neural Syst. Rehabil. Eng.*, vol. 15, no. 3, pp. 379–386, Sep. 2007, doi: 10.1109/TNSRE.2007.903919.

[12] Q. Van Tran, S. Kim, K. Lee, S. Kang, and J. Ryu, "Force/torque sensorless impedance control for indirect driven robot-aided gait rehabilitation system," in *Proc. IEEE Int. Conf. Adv. Intell. Mechatronics (AIM)*, Busan, South Korea, Jul. 2015, pp. 652–657.

[13] P. Metrailler, V. Blanchard, I. Perrin, R. Brodard, R. Frischknecht, C. Schmitt, J. Fournier, M. Bouri, and R. Clavel, "Improvement of rehabilitation possibilities with the MotionMaker^{TM}," in *Proc. 1st IEEE/RAS-EMBS Int. Conf. Biomed. Robot. Biomechatronics*, Pisa, Italy, Feb. 2006, pp. 359–364.

[14] H. Yu, S. Zheng, J. Wu, L. Sun, Y. Chen, S. Zhang, and Z. Qin, "A new single-leg lower-limb rehabilitation robot: Design, analysis and experimental evaluation," *Machines*, vol. 11, no. 4, p. 447, Apr. 2023, doi: 10.3390/machines11040447.

[15] Y. Feng, H. Wang, T. Lu, V. Vladareanuv, Q. Li, and C. Zhao, "Teaching training method of a lower limb rehabilitation robot," *Int. J. Adv. Robotic Syst.*, vol. 13, no. 2, p. 57, Mar. 2016, doi: 10.5772/62445.

[16] F. Dong, H. Li, and Y. Feng, "Mechanism design and performance analysis of a sitting/lying lower limb rehabilitation robot," *Machines*, vol. 10, no. 8, p. 674, Aug. 2022, doi: 10.3390/machines10080674.

[17] J. Zhou, R. Yang, Y. Lyu, and R. Song, "Admittance control strategy with output joint space constraints for a lower limb rehabilitation robot," in *Proc. 5th Int. Conf. Adv. Robot. Mechatronics (ICARM)*, Shenzhen, China, Dec. 2020, pp. 564–569.

[18] H. Jabbari Asl, T. Narikiyo, and M. Kawanishi, "Adaptive neural network-based saturated control of robotic exoskeletons," *Nonlinear Dyn.*, vol. 94, no. 1, pp. 123–139, Jun. 2018, doi: 10.1007/s11071-018-4348-1.

[19] Z. Chen, Q. Guo, T. Li, and Y. Yan, "Output constrained control of lower limb exoskeleton based on knee motion probabilistic model with finite-time extended state observer," *IEEE/ASME Trans. Mechatronics*, vol. 28, no. 4, pp. 2305–2316, Aug. 2023, doi: 10.1109/TMECH.2023.3235054.

[20] R. Fareh, S. Khadraoui, M. Y. Abdallah, M. Baziyad, and M. Bettayeb, "Active disturbance rejection control for robotic systems: A review," *Mechatronics*, vol. 80, Dec. 2021, Art. no. 102671, doi: 10.1016/j.mechatronics.2021.102671.

[21] Z. Gao, "Scaling and bandwidth-parameterization based controller tuning," in *Proc. Amer. Control Conf.*, Denver, CO, USA, Jun. 2003, pp. 4989–4996.

[22] Z. Shen, Y. Zhuang, J. Zhou, J. Gao, and R. Song, "Design and test of admittance control with inner adaptive robust position control for a lower limb rehabilitation robot," *Int. J. Control, Autom. Syst.*, vol. 18, no. 1, pp. 134–142, Jan. 2020, doi: 10.1007/s12555-018-0477-z.

[23] E. Akdoğan and M. A. Adli, "The design and control of a therapeutic exercise robot for lower limb rehabilitation: Physiotherabot," *Mechatronics*, vol. 21, no. 3, pp. 509–522, Apr. 2011, doi: 10.1016/j.mechatronics.2011.01.005.

[24] Y. Cao, X. Chen, M. Zhang, and J. Huang, "Adaptive position constrained assist-as-needed control for rehabilitation robots," *IEEE Trans. Ind. Electron.*, vol. 71, no. 4, pp. 4059–4068, May 2023, doi: 10.1109/TIE.2023.3273270.

[25] P. Huang, Z. Li, M. Zhou, X. Li, and M. Cheng, "Fuzzy enhanced adaptive admittance control of a wearable walking exoskeleton with step trajectory shaping," *IEEE Trans. Fuzzy Syst.*, vol. 30, no. 6, pp. 1541–1552, Jun. 2022, doi: 10.1109/TFUZZ.2022.3162700.

[26] Q. Wu and Y. Chen, "Variable admittance time-delay control of an upper limb rehabilitation robot based on human stiffness estimation," *Mechatronics*, vol. 90, Apr. 2023, Art. no. 102935, doi: 10.1016/j.mechatronics.2022.102935.

[27] W. He, C. Xue, X. Yu, Z. Li, and C. Yang, "Admittance-based controller design for physical human–robot interaction in the constrained task space," *IEEE Trans. Autom. Sci. Eng.*, vol. 17, no. 4, pp. 1937–1949, Oct. 2020, doi: 10.1109/TASE.2020.2983225.

[28] A. J. Ijspeert, J. Nakanishi, H. Hoffmann, P. Pastor, and S. Schaal, "Dynamical movement primitives: Learning attractor models for motor behaviors," *Neural Comput.*, vol. 25, no. 2, pp. 328–373, Feb. 2013, doi: 10.1162/NECO_a_00393.

[29] J. Nielsen, A. S. Sørensen, T. S. Christensen, T. R. Savarimuthu, and T. Kulvicius, "Individualised and adaptive upper limb rehabilitation with industrial robot using dynamic movement primitives," in *Proc. Workshop Adv. Challenges Develop., Test. Assessment Assistive Rehabil. Robots, Experiences Eng. Human Sci. Res.*, vol. 1, 2017, p. 40.

[30] A. Gams, B. Nemec, A. J. Ijspeert, and A. Ude, "Coupling movement primitives: Interaction with the environment and bimanual tasks," *IEEE Trans. Robot.*, vol. 30, no. 4, pp. 816–830, Aug. 2014, doi: 10.1109/TRO.2014.2304775.

[31] H. Peng, J. Zhou, and R. Song, "A triple-step controller with linear active disturbance rejection control for a lower limb rehabilitation robot," *Frontiers Neurorobot.*, vol. 16, Nov. 2022, Art. no. 1053360, doi: 10.3389/fnbot.2022.1053360.

[32] K. Gui, H. Liu, and D. Zhang, "A practical and adaptive method to achieve EMG-based torque estimation for a robotic exoskeleton," *IEEE/ASME Trans. Mechatronics*, vol. 24, no. 2, pp. 483–494, Apr. 2019, doi: 10.1109/TMECH.2019.2893055.

[33] B. Corteville, E. Aertbelien, H. Bruyninckx, J. de Schutter, and H. van Brussel, "Human-inspired robot assistant for fast point-to-point movements," in *Proc. IEEE Int. Conf. Robot. Autom.*, Roma, Italy, Apr. 2007, pp. 3639–3644.

[34] N. Sánchez, A. M. Acosta, R. Lopez-Rosado, A. H. A. Stienen, and J. P. A. Dewald, "Lower extremity motor impairments in ambulatory chronic hemiparetic stroke: Evidence for lower extremity weakness and abnormal muscle and joint torque coupling patterns," *Neurorehabilitation Neural Repair*, vol. 31, no. 9, pp. 814–826, Aug. 2017, doi: 10.1177/1545968317721974.

[35] S. Yang, J. Han, L. Xia, and Y.-H. Chen, "An optimal fuzzy-theoretic setting of adaptive robust control design for a lower limb exoskeleton robot system," *Mech. Syst. Signal Process.*, vol. 141, Jul. 2020, Art. no. 106706, doi: 10.1016/j.ymssp.2020.106706.

[36] R. Pérez-San Lázaro, I. Salgado, and I. Chairez, "Adaptive sliding-mode controller of a lower limb mobile exoskeleton for active rehabilitation," *ISA Trans.*, vol. 109, pp. 218–228, Mar. 2021, doi: 10.1016/j.isatra.2020.10.008.

[37] J. Wu, J. Gao, R. Song, R. Li, Y. Li, and L. Jiang, "The design and control of a 3DOF lower limb rehabilitation robot," *Mechatronics*, vol. 33, pp. 13–22, Feb. 2016, doi: 10.1016/j.mechatronics.2015.11.010.

[38] M. Khamar, M. Edrisi, and S. Forghany, "Designing a robust controller for a lower limb exoskeleton to treat an individual with crouch gait pattern in the presence of actuator saturation," *ISA Trans.*, vol. 126, pp. 513–532, Jul. 2022, doi: 10.1016/j.isatra.2021.08.027.
[39] P. Li, L. Wang, B. Zhong, and M. Zhang, "Linear active disturbance rejection control for two-mass systems via singular perturbation approach," *IEEE Trans. Ind. Informat.*, vol. 18, no. 5, pp. 3022–3032, May 2022, doi: 10.1109/TII.2021.3108950.
[40] Y. Zhuang, S. Yao, C. Ma, and R. Song, "Admittance control based on EMG-driven musculoskeletal model improves the human–robot synchronization," *IEEE Trans. Ind. Informat.*, vol. 15, no. 2, pp. 1211–1218, Feb. 2019, doi: 10.1109/TII.2018.2875729.
[41] Y. Zhuang, Y. Leng, J. Zhou, R. Song, L. Li, and S. W. Su, "Voluntary control of an ankle joint exoskeleton by able-bodied individuals and stroke survivors using EMG-based admittance control scheme," *IEEE Trans. Biomed. Eng.*, vol. 68, no. 2, pp. 695–705, Feb. 2021, doi: 10.1109/TBME.2020.3012296.
[42] W. Zhong, X. Fu, and M. Zhang, "A muscle synergy-driven ANFIS approach to predict continuous knee joint movement," *IEEE Trans. Fuzzy Syst.*, vol. 30, no. 6, pp. 1553–1563, Jun. 2022, doi: 10.1109/TFUZZ.2022.3158727.
[43] J. Zhou, H. Peng, M. Zheng, Z. Wei, T. Fan, and R. Song, "Trajectory deformation-based multi-modal adaptive compliance control for a wearable lower limb rehabilitation robot," *IEEE Trans. Neural Syst. Rehabil. Eng.*, vol. 32, pp. 314–324, 2024, doi: 10.1109/tnsre.2023.3348332.
[44] J. Xu, Y. Li, L. Xu, C. Peng, S. Chen, J. Liu, C. Xu, G. Cheng, H. Xu, Y. Liu, and J. Chen, "A multi-mode rehabilitation robot with magnetorheological actuators based on human motion intention estimation," *IEEE Trans. Neural Syst. Rehabil. Eng.*, vol. 27, no. 10, pp. 2216–2228, Oct. 2019, doi: 10.1109/TNSRE.2019.2937000.
[45] T. Yang, N. Sun, and Y. Fang, "Neuroadaptive control for complicated underactuated systems with simultaneous output and velocity constraints exerted on both actuated and unactuated states," *IEEE Trans. Neural Netw. Learn. Syst.*, vol. 34, no. 8, pp. 4488–4498, Aug. 2021, doi: 10.1109/TNNLS.2021.3115960.

JIE ZHOU received the B.Eng. degree in mechanical engineering from Jiangxi University of Science and Technology, Jiangxi, China, in 2015, the M.S. degree in mechanical design and theory from Northeastern University, Shenyang, China, in 2018, and the Ph.D. degree in biomedical engineering from Sun Yat-sen University, Guangzhou, China, in 2022.

He studied with the Laboratory of Space Automation Technology, Shenyang Institute of Automation, Chinese Academy of Sciences, from 2016 to 2017. He is currently a Postdoctoral Researcher with the School of Mechanical Engineering, Shenyang University of Technology, China. His research interests include rehabilitation robot design, intelligent control, physical human–robot interaction, musculoskeletal modeling, and rehabilitation evaluation.

YAO SUN received the M.S. degree in mechanical engineering and the Ph.D. degree in mechanical design and theory from Northeastern University, Shenyang, China, in 2018 and 2023, respectively. She is currently a Postdoctoral Researcher with the School of Mechanical Engineering, Shenyang University of Technology, Shenyang. Her research interests include rehabilitation robot design, biomedical signal processing, system reliability evaluation, and maintenance decisions.

RONG SONG received the B.Eng. degree in electrical engineering from Tsinghua University, in 1999, the M.S. degree in electronic engineering from Shantou University, in 2002, and the Ph.D. degree in biomedical engineering from The Hong Kong Polytechnic University, in 2006.

He is currently a Professor with the School of Biomedical Engineering, Sun Yat-sen University, China. His research interests include musculoskeletal modeling, human motion analysis, robot-assisted stroke rehabilitation, human–robot interaction, biomedical signal processing, and rehabilitation evaluation.

ZHE WEI received the B.S. degree in industrial design from Northeastern University, Shenyang, China, in 2004, and the M.S. and Ph.D. degrees in mechanical design and theory from Zhejiang University, Hangzhou, China, in 2009.

He was the Dean of the Research Institute and the Chief Process Information Officer with Sany Heavy Equipment Company Ltd., from 2009 to 2014. From 2014 to 2018, he was an Associate Professor with the State Key Laboratory of Synthetical Automation for Process Industries, Northeastern University. He is currently a Professor with the School of Mechanical Engineering, Shenyang University of Technology, Shenyang, and the Director of the Key Laboratory of Intelligent Manufacturing and Industrial Robotics in Liaoning Province. His current research interests include human–robot interaction, virtual reality, digital twins, and intelligent design and manufacturing.